Journal of the Ceramic Society of Japan 116 [6] 727-731 2008 **Paper**

Spark plasma sintering of Si_3N_4–B_4C composites

E. AYAS,† A. KALEMTAS, G. ARSLAN, A. KARA and F. KARA

Department of Materials Science & Engineering, Anadolu University, Eskisehir, Turkey

In this study the production of Si_3N_4–B_4C composites using spark plasma sintering technique was studied. This technique was preferred in order to minimize the reactions between starting constituents. Fully dense Si_3N_4 ceramic was obtained by SPS. The bulk densities of all the produced composites was found to be significantly less than that of Si_3N_4, and this was attributed to the formation of the relatively low-density reaction products. In the B_4C-containing composites there was a trend for the bulk density to increase slightly with decreasing particle size of B_4C powder. Composites containing both B_4C and TiO_2 had somewhat higher bulk densities when compared with those just containing B_4C. This was related to the formation of relatively high-density reaction products in significant amounts. The fine B_4C added to the Si_3N_4 base composition containing Al_2O_3 and Y_2O_3 as sintering additives, even when incorporated in significant amounts, was consumed readily during the fast sintering process. Using coarse B_4C particles reduced the reaction kinetics to some extent. As a result of reactions between Si_3N_4 and B_4C particles SiC, h-BN and metallic Si were formed. When both B_4C and TiO_2 were added together additional phases of Ti (C, N) and TiB_2 were formed. Possible reactions that explain the formation of the in-situ phases were proposed through thermodynamic considerations.

Key-words : Silicon nitride, Boron carbide, Spark plasma sintering, Thermodynamic consideration, In-situ formation

[Received February 17, 2008; Accepted May 15, 2008]

1. Introduction

In Si_3N_4 based systems several reinforcement phases are introduced in order to improve specific properties like mechanical, electrical and thermal. Different preparation routes have been tried such as direct incorporation of secondary phases with composite approach and introducing chemical precursors to promote in-situ formation of desired phases.[1)]

Due to its favorable properties, B_4C has been used in special applications. Properties like high melting temperature (2447°C), low density (2.52 g/cm^3), high hardness (3770 kg/mm^2), high electrical conductivity (0.1–10 Ω.cm) and the high-temperature thermoelectric properties make this material suitable for high performance applications.[2)–5)] However, it is difficult to obtain fully dense B_4C materials due to its highly covalent character. Sintering near the melting point results in abnormal grain growth and a relatively low bulk density (< 80% of theoretical value).[6)–9)] Pressure assisted sintering techniques such as hot pressing and hot isostatic pressing are widely used to obtain dense sintered bodies. However, the sintering temperature of monolithic B_4C is usually above 2200°C.[10)] Use of B_4C in ceramic matrix composites as a secondary phase is limited due to its low densification behavior.[7)] In addition, due to its chemical instability with oxide materials, reactions leading to the formation of new compounds may take place.[11)] For instance, B_4C may react with TiO_2 at high temperatures to form B_2O_3 and TiB_2.[12)] According to Kristic et al.,[10)] fully dense B_4C–TiB_2 composites can be obtained via the reactive sintering of a mixture of B_4C, TiO_2 and carbon at 1900°C.

Spark plasma sintering (SPS) technique has advantages over conventional sintering techniques like hot pressing and hot isostatic pressing, since the whole process can be completed in a few minutes, thus minimizing the reactions between constituents.[13)] Hence, this technique was preferred in the present work with the hope to minimize reactions between Si_3N_4 and B_4C. Furthermore, to the author's knowledge, a thermodynamic approach to explain the formation of the observed in-situ phases in the Si_3N_4–B_4C system has not yet been explored.

2. Experimental procedure

α-Si_3N_4 (SN E–10, Ube Ind. Ltd., < 200 nm), Y_2O_3 (Shin-Etsu Chemical Co., Ltd., 100–300 nm), Al_2O_3 (Sumitomo Chemical Co., AKP 30 grade, < 1 μm), fine B_4C (Alfa Aesar, 2 μm), coarse B_4C (Alfa Aesar, 47 μm) and TiO_2 (Merck, 20 nm) powders were used as the starting materials. Both fine and coarse as-received B_4C powders were passivated under Ar gas atmosphere at 1400°C for 4 h prior to use.[14)] The compositions of the prepared powder mixtures are given in **Table 1**. Compositions were mixed by wet milling in a planetary ball mill (Pulverisette, P5 Model) in isopropanol for 2 h using Si_3N_4 media. Prepared slurry was dried in a rotary evaporator (Heidolph WB2000, Germany) at 55°C.

Sintering of the powder mixtures was carried out at 1700°C under a uniaxial pressure of 50 MPa and under vacuum atmosphere in a SPS furnace (FCT GmbH, Germany). Powder mixtures were put into a 20 mm graphite die and a graphite foil was incorporated to prevent reaction between the graphite die and the

Table 1. Compositions of Designed Si_3N_4–B_4C Composites

Designation	Si_3N_4 mass%	Fine B_4C mass%	Coarse B_4C mass%	Al_2O_3 mass%	Y_2O_3 mass%	TiO_2 mass%
SN	92	–	–	2	6	–
SN–fB	62	30	–	2	6	–
SN–cB	62	–	30	2	6	–
SN–fBT	52	30	–	2	6	10
SN–cBT	52	–	30	2	6	10

† Corresponding author: E. Ayas; E-mail: erayas@anadolu.edu.tr

powder mixtures. Heating rate was 100°C/min. The temperature was increased with a controlled electric current and measured on the graphite die surface with an optical pyrometer. The specimens were held at the maximum sintering temperature for 5 min. Fast cooling was achieved by switching the power off.

Bulk densities of the samples were determined by the Archimedes method. Sintered samples were crushed and ground down to 50 μm for XRD analysis. Qualitative phase analysis was accomplished by using a Rigaku Rint 2200 series X-ray diffractometer at a scan speed of 1°/min. Depending on the XRD results obtained the possible reaction sequences were predicted by using the MTDATA (version 4.74). Polished and fractured surfaces of the composites were examined after gold coating using a scanning electron microscope (Supra 50 VP, Zeiss, Germany) equipped with an EDX detector. Electrical resistivity measurements of the produced composites were carried out by the two probe DC method at room temperature on disc shaped samples. Gold electrodes were deposited on both sides of the samples. The volume resistivity of the composites was measured by using a Keithley 6517A electrometer/high resistance meter.

3. Results and discussions

3.1. Characterization

Measured bulk density and open porosity contents of the produced composites are given in **Table 2**.

Table 2 indicates that fully dense Si_3N_4 was obtained by SPS method at 1700°C. Microstructural investigations carried out on fractured (**Fig. 1**a) and polished surfaces (Fig. 1b) of the reference SN confirmed the bulk density measurements revealed that a very fine (grain size, < 1 μm) and homogenous microstructure was achieved due to the fast sintering cycle. Phase analysis of SN showed that only α and β-Si_3N_4 phases were present (**Fig. 2**).

The bulk density of all the produced composites was found to be significantly less than that of Si_3N_4 material, which can be attributed to the formation of relatively low-density reaction products, h-BN and Si (**Table 3**).

B_4C-containing composites

The fracture surfaces of the B_4C-containing composites, SN–fB and SN–cB, given in **Fig. 3**, demonstrate that there is no significant difference in porosity content, in agreement with the porosity data presented in Table 2.

A representative SEM image and a typical XRD pattern of the composite SN–fB is given in **Figs. 4** and **5**, respectively. Comparison of these Figs. with those of Si_3N_4 (Figs. 1 and 2) reveals significant differences in terms of both microstructure and phase composition. The coarser grain size of the latter composite is nicely depicted in Fig. 4b.

XRD results confirmed that appreciable in-situ reactions took place in B_4C-containing samples during the sintering process, leading to the formation of new phases such as Si, SiC, and h-BN (Fig. 3&5). The presence of fine B_4C particles in the microstructure could not be verified by EDX, even though results of XRD analysis support their existence in the final composite. The formation of boron and carbon containing in-situ phases confirmed the extensive consumption of B_4C particles during the sintering process. This may be explained by the fact that the in-situ reactions possibly lead to a reduction of the fine B_4C particles to submicron size, making their detection by SEM hardly possible.

Table 2. Bulk Density and Open Porosity Contents of Composites

Designation	Bulk Density (g/cm^3)	Open Porosity (%)
SN	3.24	0.1
SN–fB	2.55	1.24
SN–cB	2.32	1.53
SN–fBT	2.66	0.69
SN–cBT	2.63	0.89

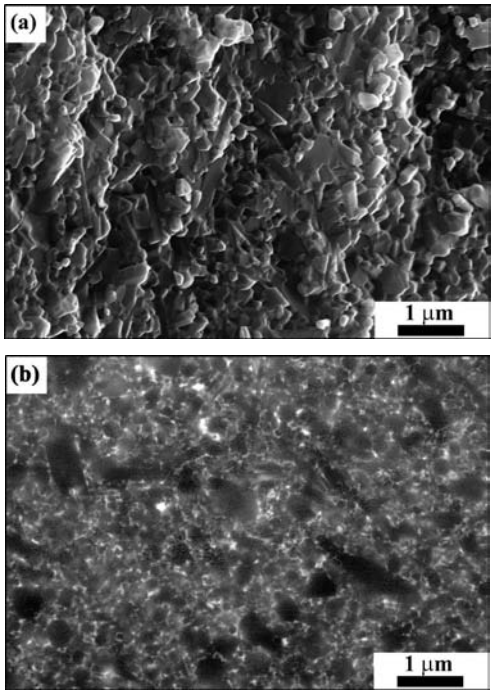

Fig. 1. Representative SEM images of Si_3N_4 (a) fractured and (b) polished surface.

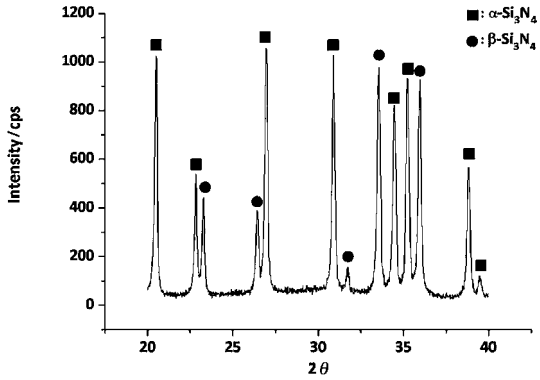

Fig. 2. X-ray diffraction pattern of Si_3N_4 sintered at 1700°C.

Table 3. Theoretical Density of Starting Materials and Reaction Products

Starting Materials	Theoretical Density (g/cm^3)	Reaction Products	Theoretical Density (g/cm^3)
Si_3N_4	3.18	h-BN	2.1
B_4C	2.52	Si	2.33
TiO_2	4.35	SiC	3.22
		TiB_2	4.50
		Ti (C, N)	5.25

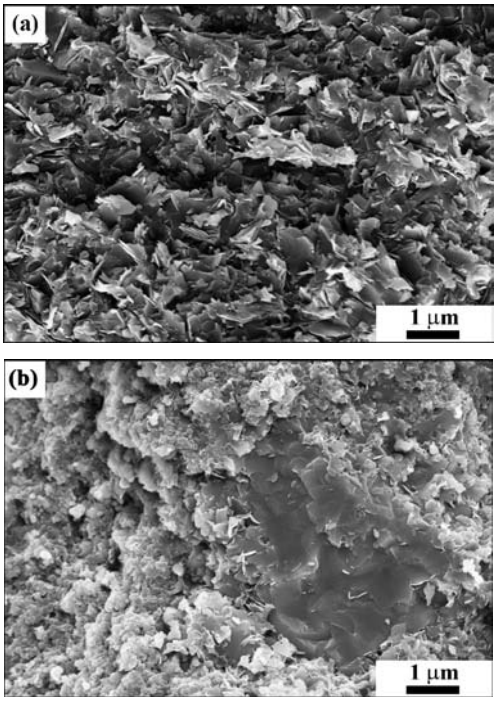

Fig. 3. Representative fracture surfaces of (a) SN–fB and (b) SN–cB.

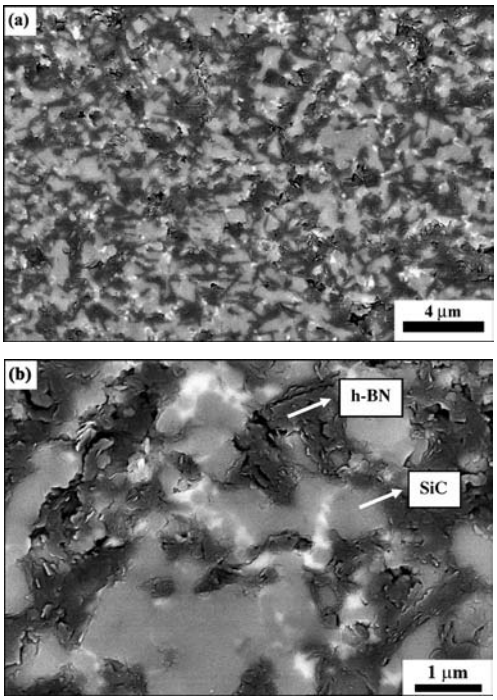

Fig. 4. Representative SEM image of composite containing fine B_4C (SN–fB).

On the other hand, the presence of partially dissolved B_4C particles (dark gray phase) in SN–cB is supported by SEM (**Fig. 6**), and XRD analysis (**Fig. 7**), respectively. It is also seen in Fig. 6 that particle size of initially coarse B_4C powders decreased sharply from ~47 μm to ~5–10 μm, due to the above mentioned in-situ reactions. When the XRD patterns of the composites produced from fine (SN–fB) and coarse (SN–cB) B_4C powders are compared it becomes apparent that the amount of in-situ h-BN

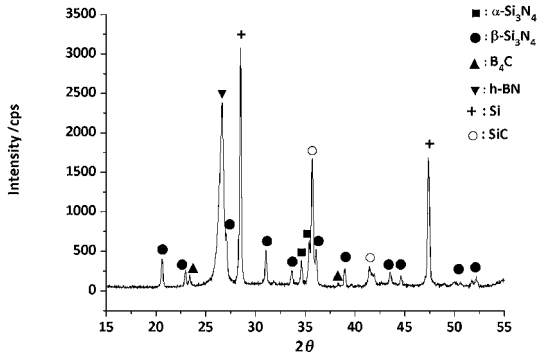

Fig. 5. X-ray diffraction pattern of composite containing fine-B_4C (SN–fB).

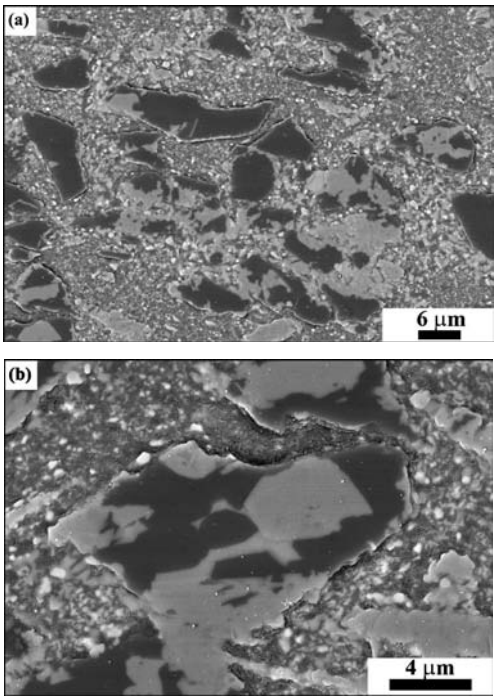

Fig. 6. Representative SEM image of composite containing coarse B_4C (SN–cB).

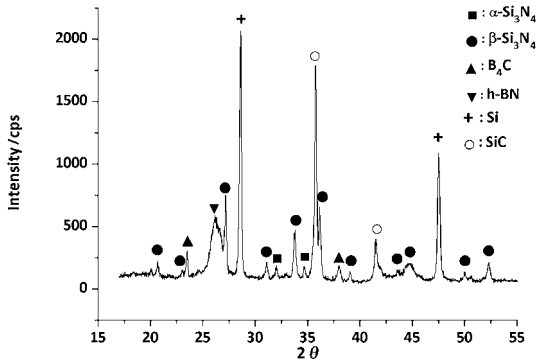

Fig. 7. X-ray diffraction pattern of composite containing coarse-B_4C (SN–cB).

produced in the latter composite (Fig. 7) is significantly less than that in the former one (Fig. 5). This may be attributed to the decrease in the reaction kinetics due to much lower surface area

of the coarse B_4C powder. Fig. 6 also infers that SiC crystals first nucleate at the rim of B_4C particles and then grow inwards.

There was a trend for the bulk density to increase slightly with decreasing particle size of B_4C powder (Table 3). The somewhat lower bulk density of the composite SN–cB (2.32 g/cm^3) relative to that of SN–fB (2.55 g/cm^3) can be explained by referring to and comparing the SEM micrographs shown in Figs. 3, 4 and 6). While in the SN–fB composite almost all B_4C powder has been consumed and resulted in the formation of somewhat higher amount of low-density h-BN formation (Figs. 3a and 4), a noticeable amount of the relatively low-density B_4C phase remains unreacted in the SN–cB composite (Fig. 6).

Composites containing both B_4C and TiO_2

When both B_4C and TiO_2 were added to the Si_3N_4 base composition (composites SN–fBT and SN–cBT), it was realized that the in-situ phases TiB_2 and Ti (C, N) formed additionally. The presence of these phases was confirmed by XRD (**Fig. 8**), SEM (**Fig. 9**) and EDX (**Fig. 10**) analyses.

The fracture surfaces of the composites containing both B_4C and TiO_2, SN–fBT and SN–cBT, given in **Fig. 11**, revealed that there was no significant difference in porosity content, in agreement with the porosity data presented in Table 2.

The data in Table 2 also indicate that the TiO_2-containing composites, SN–fBT and SN–cBT, have somewhat higher bulk density when compared with those devoid of TiO_2. This may be attributed mainly to the formation of significant amounts of the relatively high-density TiB_2 phase (Table 3, and Figs. 8, 9 and 10a). Even in less amounts, another high-density phase, Ti (C, N), is also observed to form in these composites (Table 3, and Figs. 8, 0 and 10b).

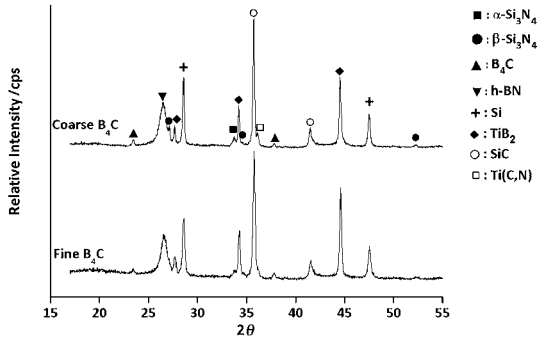

Fig. 8. Comparative X-ray diffraction pattern of composites containing both B_4C and TiO_2.

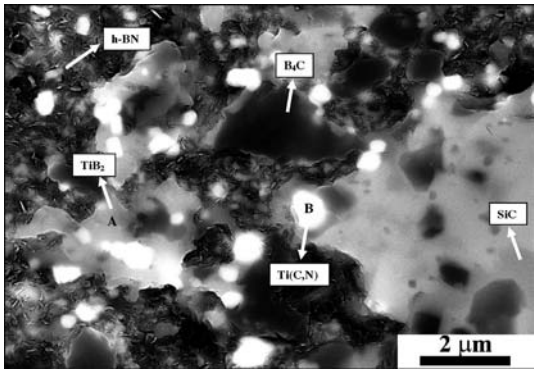

Fig. 9. Representative SEM image of composite containing fine B_4C and TiO_2 (SN–fBT).

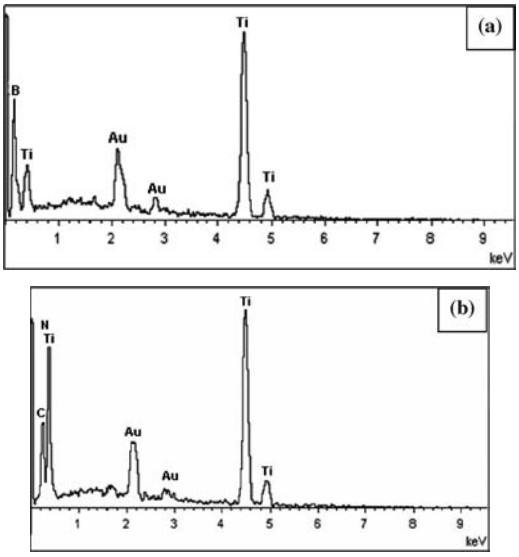

Fig. 10. EDX analysis of (a) particle A (TiB_2) and (b) particle B [Ti (C, N)] shown in Fig. 9.

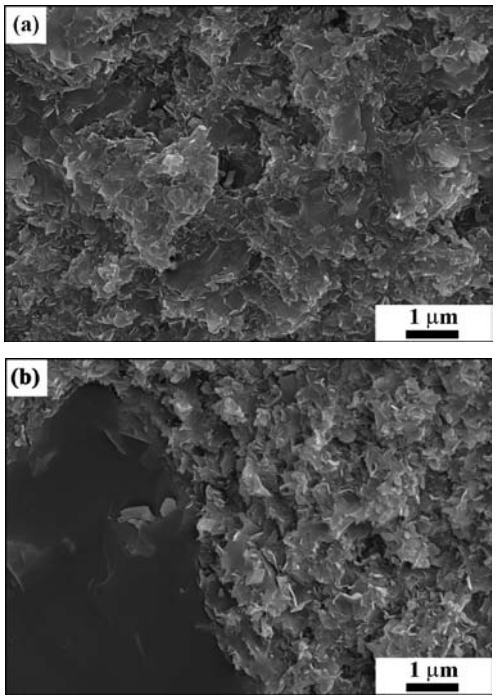

Fig. 11. Representative fracture surfaces of (a) SN–fBT and (b) SN–cBT.

3.2. Thermodynamic considerations

Based on these experimental findings and thermodynamic considerations it is proposed that in-situ reactions take place in two main steps.

In the first step, the surface oxide layers on the starting constituents are removed. The SiO_2 layer on Si_3N_4 powder is consumed by reacting with the sintering aids ($Al_2O_3 + Y_2O_3$) to form a glassy phase. Similarly, the B_2O_3 layer on B_4C may be consumed via reaction (1) to form SiO_2 and h-BN as given below.

$$B_2O_{3(l)} + \frac{1}{2}Si_3N_{4(s)} \Rightarrow 2\,BN(s) + \frac{3}{2}SiO_{2(s)}$$
$$\Delta G^\circ_{480^\circ C} \cong (-)\ 185.5\ \text{kJ/mol} \qquad (1)$$

$$\Delta G^{\circ}_{1700^{\circ}C} \cong (-)\ 139.9\ \text{kJ/mol}$$

At first glance, it may appear that the volatile B_2O_3 phase may completely leave the system during sintering in the vacuum atmosphere before having the opportunity to react with other phases. However, the relatively high boiling point of B_2O_3 (1860°C), the large thermodynamic driving force of liquid B_2O_3 to react with Si_3N_4 even at temperatures as low as ~480°C, and the formation of flakey h-BN, as verified by Figs. 4 and 5, strongly supports the occurrence of reaction (1). The formation of h-BN through nitridation of the surface B_2O_3 layer, initially present on B_4C, has to be ruled out due to the positive ΔG° value of reaction (2).

$$B_2O_{3(l)} + N_{2(g)} \Rightarrow 2BN_{(s)} + \frac{3}{2}O_{2(g)}$$
$$\Delta G^{\circ}_{1700^{\circ}C} \cong 711.9\ \text{kJ/mol} \qquad (2)$$

In step two, the surface oxide free starting constituents may react with each other and result in the formation of new phases.

3.2.1 Si_3N_4–B_4C system

In the Si_3N_4–B_4C system, the surface oxide-free B_4C and Si_3N_4 particles, react with each other to form the in-situ phases BN, SiC and Si through the suggested reaction given below.

$$Si_3N_{4(s)} + B_4C_{(s)} \Rightarrow 4BN_{(s)} + SiC_{(s)} + Si_{(l)}$$
$$\Delta G^{\circ}_{1700^{\circ}C} \cong (-)\ 249.5\ \text{kJ/mol} \qquad (3)$$

The validity of reaction (3) is confirmed by the presence of h-BN, SiC and Si (Figs. 4–7).

In this study, liquid phase sintering was achieved via consolidation of designed compositions. Thus, there is always an oxygen-containing liquid phase at the grain boundaries. Therefore, some complementary reactions (Eqs. 4–6) that may take place between B_4C and Si_3N_4 at 1700°C are to be considered as well. From the ΔG° values of these reactions it becomes apparent that they all have a strong driving force to take place spontaneously.

$$Si_3N_{4(s)} + B_4C_{(s)} + 2\ O_{2\,(g)} \Rightarrow 4\ BN_{(s)} + 2\ SiO_{2(s)} + SiC_{(s)} \qquad (4)$$
$$\Delta G^{\circ}_{1700^{\circ}C} \cong (-)\ 1562.6\ \text{kJ/mol}$$

$$SiO_{2(s)} + B_4C_{(s)} + 2\ O_{2\,(g)} \Rightarrow SiC_{(s)} + 2\ B_2O_{3(l)}$$
$$\Delta G_{1700^{\circ}C} \cong (-)\ 1279.0\ \text{kJ/mol} \qquad (5)$$

$$Si_3N_{4(s)} + B_4C_{(s)} + O_{2\,(g)} \Rightarrow 4\ BN_{(s)} + SiO_{2(s)} + SiC_{(s)} + Si_{(l)} \qquad (6)$$
$$\Delta G_{1700^{\circ}C} \cong (-)\ 906.1\ \text{kJ/mol}$$

SiC may also form according to the reaction (7) as a result of the interaction between Si coming from the dissolution of Si_3N_4, and C coming from the dissolution of B_4C.

$$Si_{(l)} + C_{(s)} \Rightarrow SiC_{(s)}$$
$$\Delta G_{1700^{\circ}C} \cong (-)\ 47.6\ \text{kJ/mol} \qquad (7)$$

3.2.2 Si_3N_4–B_4C–TiO_2 system

Formation of h-BN, SiC and metallic Si in the composites SN–fBT and SN–cBT is considered to take place again through the previously proposed reactions (1)–(6) while the formation of TiB_2 is related to reaction (8) given below.

$$B_2O_{3(l)} + TiO_{2(s)} + Si_3N_{4(s)} + B_4C_{(s)} \Rightarrow$$
$$TiB_{2(s)} + SiC_{(s)} + 2\ SiO_{2(s)} + 4\ BN_{(s)} + \frac{1}{2}O_{2(g)} \qquad (8)$$

$$\Delta G_{1700^{\circ}C} \cong (-)\ 154.7\ \text{kJ/mol}$$

4. Summary

Fully dense ($\leq 0.1\%$) Si_3N_4 ceramic was obtained by SPS. The bulk densities of all the produced composites was found to be significantly less than that of Si_3N_4, and this was attributed to the formation of the relatively low-density reaction products h-BN and Si. Although they had somewhat higher porosity contents than the produced Si_3N_4 ceramic, the density was still above 98% of the theoretical density in all composites. TiO_2 additions decreased the porosity content to below 1%. In the B_4C-containing composites there was a trend for the bulk density to increase slightly with decreasing particle size of B_4C powder. Composites containing both B_4C and TiO_2 had somewhat higher bulk densities when compared with those just containing B_4C. This was related to the formation of relatively high-density reaction products, mainly TiB_2, in significant amounts in the former ones.

The fine B_4C added to the Si_3N_4 base composition, even when incorporated in significant amounts, was consumed readily during the fast sintering process. The occurrence of simultaneous in-situ reactions lead to the formation of SiC, h-BN and metallic Si, during sintering. Using coarse B_4C particles reduced the reaction kinetics to some extent.

In addition to the in-situ phases observed in the composites containing fine B_4C and coarse B_4C, Ti (C, N) and TiB_2 phases were present in the composites containing both B_4C and TiO_2.

The reactions proposed all have a thermodynamic driving force to take place spontaneously and do explain the formation of the in-situ phases observed and are qualitatively in line with the experimental results obtained.

Acknowledgement The authors would like to thank to Anadolu University Research Foundation for funding the present work under a contract number of 60266.

References

1) Y. G. Gogotsi, *J. Mater. Sci*., 29, 2541 (1994).
2) M. Bougoin and F. Thevenot, *J. Mater. Sci*., 22, 109–114 (1987).
3) M. T. Spohn, *Am. Ceram. Soc. Bull*., 72, 88 (1993).
4) R. Telle, *Structure and Properties of Ceramics, Materials Science and Technology*, Vol. 11, VCH publishers, Weinheim, Germany (1994).
5) A. Weimer, *Carbide, Nitride, and Boride Materials Synthesis and Processing*, Chapman and Hall, New York, 7 (1997).
6) C. P. Cameron, Reaction Processing of AlN/B_4C Composites. US Patent No. 5258337 (1993).
7) G. Magnani, G. Beltrani, G. L. Minoccari and L. Pillotti, *J. Eur. Ceram. Soc.*, 21, 633–638 (2001).
8) G. Q. Weaver, Process for making aluminium modified boron carbide and products resulting there form. US Patent No. 4104062 (1978).
9) L. S. Sigle, *J. Eur. Ceram. Soc*., 18, 1521–1529 (1998).
10) V. V. Shorokhod, M. D. Vlajic and V. D. Kristic, *Mat. Sci. Forum*., 282–283, 219–224 (1998).
11) H. R. Baharvandi, A. M. Hadian and A. Alizadeh, *Appl Compos Mater*, 13, 191–198 (2006).
12) H. Zhao, K. Hiragushi and Y. Mizota, *J. Eur. Ceram. Soc*., 23, 1485–1490 (2003).
13) Z. A. Munir, U. Anselmi–Tamburini and M. Ohyanagi, *J. Mater Sci*., 41, 763–777 (2006).
14) A. J. Pyzik, U. V. Deshmukh, S. D. Dunmead, J. J. Ott, T. Allen and H. E. Rossow, *U.S. Patent* 5,521,016 (1996).